Abrus Agglutinin, a Type II Ribosome Inactivating Protein Inhibits Akt/PH Domain to Induce Endoplasmic Reticulum Stress Mediated Autophagy-Dependent Cell Death

Prashanta Kumar Panda,[1] Birendra Behera,[2] Biswa Ranjan Meher,[3] Durgesh Nandini Das,[1] Subhadip Mukhopadhyay,[1] Niharika Sinha,[1] Prajna Paramita Naik,[1] Bibhas Roy,[2] Joyjyoti Das,[2] Subhankar Paul,[4] Tapas K. Maiti,[2] Rajesh Agarwal,[5,6] and Sujit K. Bhutia[1]*

[1]*Department of Life Science, National Institute of Technology, Rourkela, Odisha, India*
[2]*Department of Biotechnology, Indian Institute of Technology, Kharagpur, West Bengal, India*
[3]*Department of Biochemistry, Indian Institute of Science, Bangalore, Karnataka, India*
[4]*Department of Biotechnology and Medical Engineering, National Institute of Technology, Rourkela, Odisha, India*
[5]*Department of Pharmaceutical Sciences, Skaggs School of Pharmacy and Pharmaceutical Sciences, Aurora, Colorado*
[6]*University of Colorado Cancer Center, University of Colorado Denver, Aurora, Colorado*

Abrus agglutinin (AGG), a type II ribosome-inactivating protein has been found to induce mitochondrial apoptosis. In the present study, we documented that AGG-mediated Akt dephosphorylation led to ER stress resulting the induction of autophagy-dependent cell death through the canonical pathway in cervical cancer cells. Inhibition of autophagic death with 3-methyladenine (3-MA) and siRNA of Beclin-1 and ATG5 increased AGG-induced apoptosis. Further, inhibiting apoptosis by Z-DEVD-FMK and N-acetyl cysteine (NAC) increased autophagic cell death after AGG treatment, suggesting that AGG simultaneously induced autophagic and apoptotic death in HeLa cells. Additionally, it observed that AGG-induced autophagic cell death in Bax knock down (Bax-KD) and 5-FU resistant HeLa cells, confirming as an alternate cell killing pathway to apoptosis. At the molecular level, AGG-induced ER stress in PERK dependent pathway and inhibition of ER stress by salubrinal, eIF2α phosphatase inhibitor as well as siPERK reduced autophagic death in the presence of AGG. Further, our in silico and colocalization study showed that AGG interacted with pleckstrin homology (PH) domain of Akt to suppress its phosphorylation and consequent downstream mTOR dephosphorylation in HeLa cells. We showed that Akt overexpression could not augment GRP78 expression and reduced autophagic cell death by AGG as compared to pcDNA control, indicating Akt modulation was the upstream signal during AGG's ER stress mediated autophagic cell death. In conclusion, we established that AGG stimulated cell death by autophagy might be used as an alternative tumor suppressor mechanism in human cervical cancer.

Key words: *Abrus* agglutinin; autophagic cell death; apoptosis; ER stress; Akt; PH domain

INTRODUCTION

Autophagy is an evolutionary catabolic process in which stressed cells form cytoplasmic, double-layered, crescent-shaped membranes known as phagophores, which mature into complete autophagosomes. The autophagosome engulfs damaged cytoplasmic organelles and long-lived proteins to provide cellular energy and building blocks for cellular biosynthesis [1,2]. The autophagosome fuse with lysosome to form autolysosome and cargo are digested by lysosomal hydrolases to metabolites and released back to the cytosol for recycling. The autophagic process is regulated by the *ATG* genes (autophagy-related genes) and the proteins encoded by the autophagy related genes (ATG) are required for the regulation of autophagic vesicles. Initially, the autophagic pathway functions as an adaptive response to stress. However, in the face of extreme or protracted stress, cells are committed to autophagic cell death; type II programmed cell death (PCD) [2,3].

Cervical cancer is the fourth leading cause of cancer cell death and third most commonly diagnosed cancer

Abbreviations: AGG, *Abrus* agglutinin; ROS, reactive oxygen species; ER, endoplasmic reticulum; UPR, unfolded protein response; CHOP, C/EBP homologous protein; GRP94, glucose-regulated protein 94; eIF2α, eukaryotic initiation factor 2 subunit α; ERAD, ER-associated ubiquitin/proteasome degradation; MD, molecular dynamics; PDB, protein data bank; MM-PB/GBSA, molecular mechanics Poisson–Boltzmann/generalized born surface area.

Grant sponsor: Council of Scientific and Industrial Research (CSIR); Grant number: 37(1608)/13/EMR-II; Grant sponsor: Department of Biotechnology; Grant number: BT/PR1/5090/GBD/27/309/2011; Grant sponsor: Science and Engineering Research Board (SERB); Grant number: SR/SO/BB-0101/2012; Grant sponsor: NCI R01, United States; Grant number: CA195708

*Correspondence to: Department of Life Science, National Institute of Technology, Rourkela 769008, Odisha, India.

Received 9 November 2015; Revised 26 April 2016; Accepted 13 May 2016

DOI 10.1002/mc.22502

Published online in Wiley Online Library (wileyonlinelibrary.com).

in women worldwide. Of these, nearly 85% of cases occur in developing countries including India, and other parts of Asia due to inadequate access to screening services and lack of human papillomavirus (HPV) vaccination [4,5]. In the era of cancer therapy, apoptosis induction in tumor cells is increasingly seen as prime candidates for the development of anticancer therapeutics for cervical cancer. However, development of resistance phenomena to apoptosis and ineffectiveness of single treatment modality allow cancer cells to survive, consequently escape current cancer therapy. Therefore, novel therapeutic strategies are needed to enhance the effect of cancer therapy as well as address the emerging problem of drug resistance. Induction of autophagic death, a type II programmed cell death, could be a potentially useful therapeutic approach in apoptosis resistant cancer cells and could complement as a multiple treatment approaches along with apoptosis in apoptosis undergoing cancer cells [1,6]. Moreover because cancer cells often display defective apoptotic propensity, autophagy is considered a tumor suppressor mechanism. As an alternative therapy for cancer, recently more efforts are made for the development of novel molecules that specifically targets the autophagic cell death mechanism [7–9].

Abrus agglutinin (AGG) is one such prime candidate whose autophagic attributes are being documented in this work. AGG isolated from the seeds of *A. precatorius* is a hetero-tetrameric glycoprotein of 134-kDa molecular weight, composed of two A and two B chains linked through disulfide bridges. AGG has specificity towards [gal(β1→3)galNAc] and belongs to type II ribosome inactivating protein family (RIP II) with a protein synthesis inhibitory concentration (IC_{50}) of 0.469 μg/ml and a lethal dose (LD_{50}) 5 mg/kg body weight in mice [10,11]. AGG contains cytotoxic A chain having ribosomal RNA N-glycosidase activity which cleaves glycosidic bond at position A-4324 within the universally conserved α-sarcin loop of the 28S ribosomal RNA of eukaryotes while the B chain binds to carbohydrate moieties on the cell surface and facilitates the internalization of the entire toxin into the cell [12]. Our groups have previously elucidated the anticancer effects of AGG in several tumor models at sublethal doses by direct killing of tumor cells through extrinsic and intrinsic apoptosis [13–15]. Along with direct antitumor potential, AGG generates potent humoral and cellular immune responses in normal as well as tumor-bearing animals [16–18]. The adjuvant property of AGG is reported in oil emulsion and aqueous solution for potentiating the systemic immune response [19]. AGG activates splenocytes and induces production of Th1 type of immune response. Further, AGG stimulates the innate effector arms like macrophage and natural killer cells. Furthermore, heat denatured and tryptic digested AGG show potent antitumor as well as immunomodulatory activity in normal as well as tumor bearing mice [11,17,20,21].

Although the apoptotic potential of AGG has been extensively investigated and well characterized, its ability to induce autophagy-dependent cell death in mammalian cells has not been documented. In this report, the study was designed to decipher the role of AGG in autophagic death and discuss the possible role of autophagic death in relation with apoptosis in HeLa cells. Further, we examined that AGG inhibited Akt/PH domain to induce endoplasmic reticulum stress mediated autophagy-dependent cell death.

MATERIALS AND METHODS

Reagents

4′,6-Diamidino-2-phenylindole dihydrochloride (DAPI), Dihydrorhodamine 123, propidium iodide (PI), 3-[4,5-Dimethylthiazol-2-yl]-2,5-diphenyltetrazolium (MTT), dimethylsulfoxide (DMSO), Caspase inhibitor Z-DEVD-FMK, 3-methyl adenine (3 MA), N-Acetyl-L-cysteine (NAC), 5-fluorouracil (5-FU), and agarose were purchased from Sigma–Aldrich (St. Louis, MO). Minimal essential medium (MEM), Fetal bovine serum (FBS) (sterile-filtered, South American origin), Dulbecco's minimal essential medium (DMEM), antibiotic-antimycotic (100×) solution, Lyso Tracker red, ER-Tracker Green, and Lipofectamine 2000® were purchased from Invitrogen (Waltham, MA). Salubrinal obtained from Millipore (Billerica, MA).

Antibodies

LC3 (NB100-2220) from Novus Biological (Littleton, CO); Phospho-mTOR (Ser2448) (2971), mTOR (2983), Beclin-1 (3738S), Atg5 (2630S), PARP (9542S), Akt (pan) (4691S), Phospho-Akt (Ser473) (4060S), Bax (2772BC), Phospho eIF2α (Ser 51) (9721S), GRP94 (2104BC), CHOP (5554BC), and PERK (3192) from Cell Signaling Technologies (Danvers, MA); GRP78 (610978), p62 (610832) from BD Biosciences (Franklin Lakes, NJ); Phospho-PERK (Thr 981) (sc-32577), si PERK (sc-36213), and ATF6 (sc-22799) were procured from Santa Cruz (Dallas, TX); β-actin (A5316) was purchased from Sigma (St. Louis, MO).

Purification of AGG

Purification of AGG was carried out according to previously reported method. Crude extract of *Abrus precatorius* seed kernels were extracted with 30–90% ammonium sulfate precipitation followed by affinity chromatography using lactamyl Sephadex-G-100 affinity column. Purified AGG from *Abrus* abrin was obtained performing Sephadex-G-100 gel permeation chromatography using FPLC. Lectin activity of AGG was analyzed by Haemagglutination assay and purity of AGG was checked by SDS and Native PAGE analysis [10].

Cell Culture

Human cervical cancer cell lines HaCaT, HeLa, SiHa, and CaSki were obtained from the National Centre for

Cell Science, Pune, India. HeLa, SiHa were cultured in modified eagle medium (MEM) and supplemented with antibiotic-antimitotic and 10% fetal bovine serum. CaSki cells were grown in RPMI 1640 medium supplemented with antibiotic-antimitotic and 10% fetal bovine serum. HaCaT (human keratinocyte cell line) were maintained in Dulbecco's modified Eagle medium (DMEM) containing similar supplements. After that, all cells were incubated at 37°C in a humidified 95% air, 5% CO_2 incubator. The 5-FU-resistant HeLa cell line was achieved by continuous stepwise exposure to 5-FU with an initial concentration of 10 μM to final 100 μM [7].

MTT Assay

Cells from the logarithmic phase were maintained in culture after that they were counted in a hemocytometer using trypan blue solution. About 5×10^4 HeLa cells/ml was incubated with various concentrations of AGG in a 96-well plate. The efficacy of AGG on the viability of various cancer cell lines was determined using MTT dye reduction assay by determining the optical density at 595 nm using a micro-plate reader spectrophotometer (Perkin-Elmer, Waltham, MA) [11].

Plasmids, Small Interfering RNA, and Transfection

HeLa cells were cultured in 60 mm Petri plate and transfected with an 80% confluency using Lipofectamine 2000 reagent (Invitrogen) following manufacturer's protocol. Transfections were done in the presence of human specific, GFP-LC3 (Addgene plasmid No-11546), Akt (Addgene plasmid No-9008), pGFP-Akt-PH (Addgene plasmid No-18836), BAX knock down (KD), vector (Addgene plasmid No-16575) as well as with an empty backbone pcDNA (Addgene plasmid No-10792) used for mock transfection. siRNA for Beclin-1 (sc29797), ATG5 (SC-41445), and PERK (sc-36213) were purchased from Santa Cruz Biotechnology. HeLa cells were transfected with specific siRNA by using Lipofectamine 2000, following the manufacturer's instructions. After 48 h of transfection cells were treated with AGG and autophagy and apoptosis were studied.

Acridine Orange Staining

Quantification of acidic organelles was done by acridine orange staining. After treatment with various doses of AGG for 24 h cells were stained with 10 mM acridine orange at 37°C in the dark for 15 min and washed twice with PBS. Images of acridine orange staining were taken immediately using a fluorescence microscope (Olympus IX71, Tokyo, Japan) [22].

Transmission Electron Microscopy

For transmission electron microscopy (TEM), HeLa cell populations were rinsed with 0.1 Sorensen's buffer (pH 7.5), fixed in 2.5% glutaraldehyde for 1.5 h, and subsequently dehydrated and embedded in Spurr's resin. The block was then sectioned into 60-100-nm ultrathin sections and picked up on copper grids. For routine analysis, ultrathin sections were stained with 2% uranyl acetate and lead citrate. Electron micrographs were obtained using a transmission electron microscope [23].

Measurement of Autophagy by GFP-LC3 Transfection

HeLa cells were transfected with pEGFP-LC3 (Addgene plasmid 11546) using Lipofectamine 2000 reagent® (Gibco) according to the manufacturer's instructions. The GFP-LC3-HeLa stable clone was generated using G418 screening. HeLa cells were treated with different doses of AGG for 24 h and analyzed by a confocal laser scanning microscope. The level of autophagy was quantified by counting the mean number of puncta displaying intense staining, and a minimum of 100 GFP-LC3-transfected cells were counted.

Western Blot Analysis

HeLa cells were treated with AGG followed by extraction of proteins. Cell extracts in cell lysis buffer were prepared, and equal amount of proteins were resolved by SDS/PAGE, transferred to PVDF membrane, and evaluated for LC3, Beclin-1, ATG5, p62, GRP78, GRP94, p-eIF2α, Akt, p-Akt, PARP, PERK, p-PERK, ATF6, Bax, actin protein level as described by Ref. [11].

Immunofluorescence Analysis

HeLa cells were treated with various doses of AGG for 24 h followed by fixation with 10% formaldehyde. Cell permeabilization was done in 0.1% Triton X 100 which followed to blocking in 5% BSA. Following this, cells were incubated with primary antibodies p-eIF2α (1:500), CHOP (1:500). Following washing in PBST cells were incubated with secondary antibodies conjugated with the Alexa Flour. Imaging was done using a high-end fluorescence inverted microscope (Olympus IX-71) using Cell Sens Standard software.

Reactive Oxygen Species (ROS) Measurement

To detect reactive oxygen species (ROS), HeLa cells were treated with AGG for 24 h and incubated with 2.5 μg/ml Dihydrorhodamine123 (Dhr123) in PBS for 30 min in a CO_2 incubator. Dhr123 is rapidly taken up by cells and is converted to rhodamine 123 in the presence of ROS. HeLa cells were harvested and suspended in PBS, and ROS generation was measured by the fluorescence intensity (FL-1, 530 nm) of 50 000 cells [11].

Colocalization Study by ER-Tracker, LysoTracker, and Mito Tracker

Cells were treated with AGG for different time intervals and stained with prewarmed ER-Tracker Green (BODIPY®FLglibenclamide) (500 nM) staining solution and were incubated for 20–30 m at 37°C. Glibenclamide attaches to the sulphonylurea receptors of ATP-sensitive K+ channels which are generally

prominently present on ER. At the same time, cells were stained with LysoTracker Red DND-99 (100 nM) for 30 m at 37°C. LysoTracker probes are specific for acidic organelles. Likewise, mitochondrial probe like MitoTracker Green (20 nM) contains a mildly thiol-reactive chloromethyl moiety used for labeling mitochondria. Colocalization of ER and lysosome was observed using ER- and Lyso-Tracker. Similarly, colocalization of mitochondria and lysosome was demonstrated for representing the selective occurrence of ER-phagy by AGG. Colocalization was measured applying JACoP plugin in single Z-stack sections of deconvoluted images.

Caspase-Glo 3/7 Assay

Caspase 3/7 activity in HeLa cells was measured using Caspase-Glo 3/7, Assay kits (Promega) according to the manufacturer's instructions. Caspase activities were measured and expressed as relative luciferase units.

RITC Labeling of AGG for Colocalization Study With Akt-PH Domain

For colocalization study, AGG were labeled with Rhodamine B isothiocyanate (RITC) dissolved in water (1 mg in 100 μl water) and 1 mg of AGG dissolved in 1 ml of 100 mM NaHCO3 buffer). After that, the mixture was incubated for 4 h in dark at room temperature followed by treatment with 1M Ethanolamine to inactivate the residual RITC. The solution was left in the dark for 2 h and dialyzed against PBS for 48 h and lyophilized. After 30 min of AGG (10 μg/ml) treatment in GFP-Akt-PH domain transfected HeLa cells, cells were washed and colocalization study was performed in confocal microscope and colocalization was measured by using JACoP plugin in single Z-stack sections of deconvoluted images [11].

Modeling PH-AGG Complex Through Docking and Molecular Dynamics Simulation

The crystal structures of the pleckstrin homology (PH) domain and AGG were obtained from the PDB with PDB ids: 2Q3N [12] for the AGG and 1UNQ [24] for the PH domain. The docking algorithm was carried out by the ClusPro 2.0 protein–protein docking server. Finally, structure with the highest score was considered for the MD simulation with the *ff12SB* force field and TIP3P waters in AMBER12 package [25–27]. The system was then minimized in four phases and equilibrated in a total of 400 ps. The PH-AGG complex trajectory was run for 15 ns and was used for the analysis. The binding free energies were calculated using the MM-PB/GBSA method implemented in AMBER 12. The MMPBSA.py method in Amber12 was applied to calculate the binding free energy of the PH domain to the AGG. The MM-PB/GBSA method can be summarized as:

$$\Delta G_{\text{bind}} = G_{\text{complex}} - G_{\text{receptor}} - G_{\text{ligand}}$$

The detailed materials and methods for in silico part were described in the Supplementary Section.

Statistical Analysis

All the results were represented as the mean ± SD. Experimental data were analyzed by Student's *t*-test. The level of significance was regarded as $P < 0.05$ for values obtained for treatment compared to control. The IC_{50} values of various cell lines after AGG treatment were calculated by using the program GraphPad Prism 5 (GraphPad Software, San Diego, CA) to fit a variable slope-sigmoidal-dose-response curve.

RESULTS

AGG-Induced Autophagic Cell Death in Cervical Carcinoma

To investigate the role of AGG on growth and proliferation of cervical cancer cells, we performed cell viability assay. AGG was treated in various concentrations in several cervical cancer cell lines and the effective concentration at which cell growth inhibited by 50% (IC_{50}) for HeLa, SiHa, and CaSki are 7.2 ± 1.2, 9 ± 3, and 10.2 ± 2.2 μg/ml, respectively. However, we did not observe any significant growth inhibitory activity of AGG in normal keratinocyte cell line (HaCaT) in comparison to cervical cancerous cell lines. This depicted the selective antitumor activity of AGG towards cervical cancer cells (Figure 1a).

In our initial experiment for detecting of the acidic vesicles, we used the lysosomotropic agent acridine orange, a weak base that moves freely across biological membranes when uncharged. The cytoplasm and the nucleus show dominant green fluorescence. Its protonated form accumulates in acidic compartments, where it forms fluorescence bright red color aggregates. The HeLa cells were incubated with different concentration of AGG for 24 h and acridine orange staining was performed to observe in a fluorescence microscope. The data showed that the acidic content as the red signal was increased in a dose depended way (Figure 1b and c). Similarly, the intracellular localization of LC3 in autophagic vacuoles induced by AGG was determined by transient transfection of HeLa cells with a plasmid expressing green fluorescent protein fused with LC3 (GFP-LC3) followed by AGG treatment. In control, GFP-LC3 was found predominantly as diffuse green fluorescence in the cytoplasm. However, in AGG treated cells, characteristic puncta fluorescent patterns were observed, indicating the recruitment of GFP-LC3 during autophagosome formation (Figure 1d, Upper panel). Moreover, the numbers of cells with GFP-LC3 puncta increased significantly in a dose-dependent manner after 24 h of AGG (Figure 1d, lower panel). We further verified AGG-induced autophagy in HeLa cells by

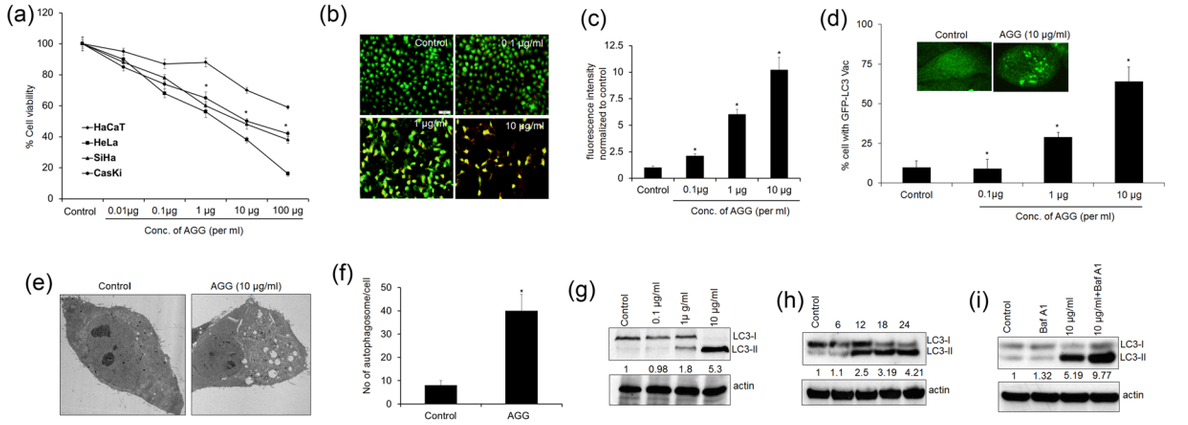

Figure 1. AGG-induced autophagic cell death in cervical cell carcinoma. The normal HaCaT cell and different cervical cell carcinoma (HeLa, SiHa, CaSki) were treated with different concentration of AGG for 72 h and cell viability was performed by MTT assay (a). HeLa cells were treated with different doses of AGG (0.1, 1, and 10 µg/ml) for 24 h, and acridine orange staining was performed for late autophagic vesicles, which were visualized with an inverted fluorescence microscope (Olympus IX71, 200×) (b). All images were quantified by using Image J (c). HeLa cells were transfected with GFP-LC3 and stable GFP-LC3-HeLa was generated and treated with different concentration of AGG for 24 h, localization of LC3 in transfected cells were examined by confocal microscopy (magnification 1000×), and autophagosome formation was quantified and data presented as percentage of GFP-LC3-transfected cells with puncta fluorescence to autophagosome formation. A minimum of 100 GFP-LC3-transfected cells were counted (d). HeLa cells were treated with different doses of AGG and cells were fixed and processed for electron microscopy (e). The numbers of autophagosomes in HeLa cells 24 h after AGG treatment was quantified (f). After 24 h of AGG treatment, LC3-II expression was analyzed by Western blot in both dose (g) and time (h) dependent manner. For the occurrence of autophagic flux, LC3-II expression was analyzed in the presence of bafilomycin A1 (100 nM) in 24 h AGG treated HeLa cells (i). The values are the means ± SD of three independent experiments. *Corresponds statistically significant change in comparison to control ($^*P < 0.05$). Densitometry was performed on the original blots, considering the ratio of LC3-II to actin in control cells was 1.

electron microscopy. Electron micrographs of control showed the normal morphology of all organelles, with mitochondria scattered homogenously throughout the cell (Figure 1e and f). Images were captured after 24 h treatment with AGG indicated marked accumulation of membrane-bound electron dense structures sequestering cellular components, a distinctive feature of autophagosomes. Furthermore, the number of autophagosomes as well as autolysosomes were increased in AGG treated cells as compared to control (Figure 1f, and Supplementary Section, Figure S1).

Next, we monitored changes in expression of endogenous LC3 in HeLa cells. Treatment of AGG led to a rapid accumulation of the LC3-II form in a dose- and time-dependent manner when compared to control cells (Figure 1g and h). The increase in LC3-II accumulation can be associated with either an enhanced formation of autophagosomes or impaired autophagosome degradation. To differentiate between these two possibilities, LC3-II accumulation was assessed in the presence of bafilomycin A1, an inhibitor of V-ATPase that interferes with the fusion of autophagosomes and lysosomes and hence blocks the autophagosome as well as LC3-II degradation. Interestingly, AGG showed further accumulation of LC3-II in the presence of bafilomycin A1 in HeLa cells. These observations suggest that the increased LC3-II association with vesicles mediated by AGG was a consequence of increased autophagosome formation (Figure 1i).

AGG-Induced Autophagic Cell Death Is Mediated Through Canonical Pathway

Autophagy can be induced by the canonical pathway in which Beclin-1 induces the autophagosome generation by forming a multiprotein complex with class III phosphatidylinositol-3-kinase or hVps34 or by the non-canonical pathway that is independent of Beclin-1 and hVps34. Initially, the expression of different types of autophagy proteins were analyzed by Western blot and showed that AGG increased the expression of Beclin-1 and ATG5 in a dose dependent manner. At the same time, p62 was degraded in the presence of AGG (Figure 2a). Further, we used a siRNA approach to knockdown essential autophagy (ATG) genes, such as Beclin-1, ATG5, and quantified LC3-II accumulation and GFP-LC3 puncta formation. The specific siRNAs significantly downregulated the expression of corresponding proteins (Figure 2b). Inhibition of Beclin-1 and ATG5 decreased the LC3-II levels and percentage of GFP-LC3-positive cells (Figure 2c and d) upon AGG treatment indicating that AGG triggered autophagic cell death via the canonical pathway.

Crosstalk Between AGG-Induced Apoptosis and Autophagy-Dependent Cell Death

To investigate the role of AGG in apoptotic and autophagic death, HeLa cell were cultured in presence of PI3K-III inhibitor, 3-methyladenine

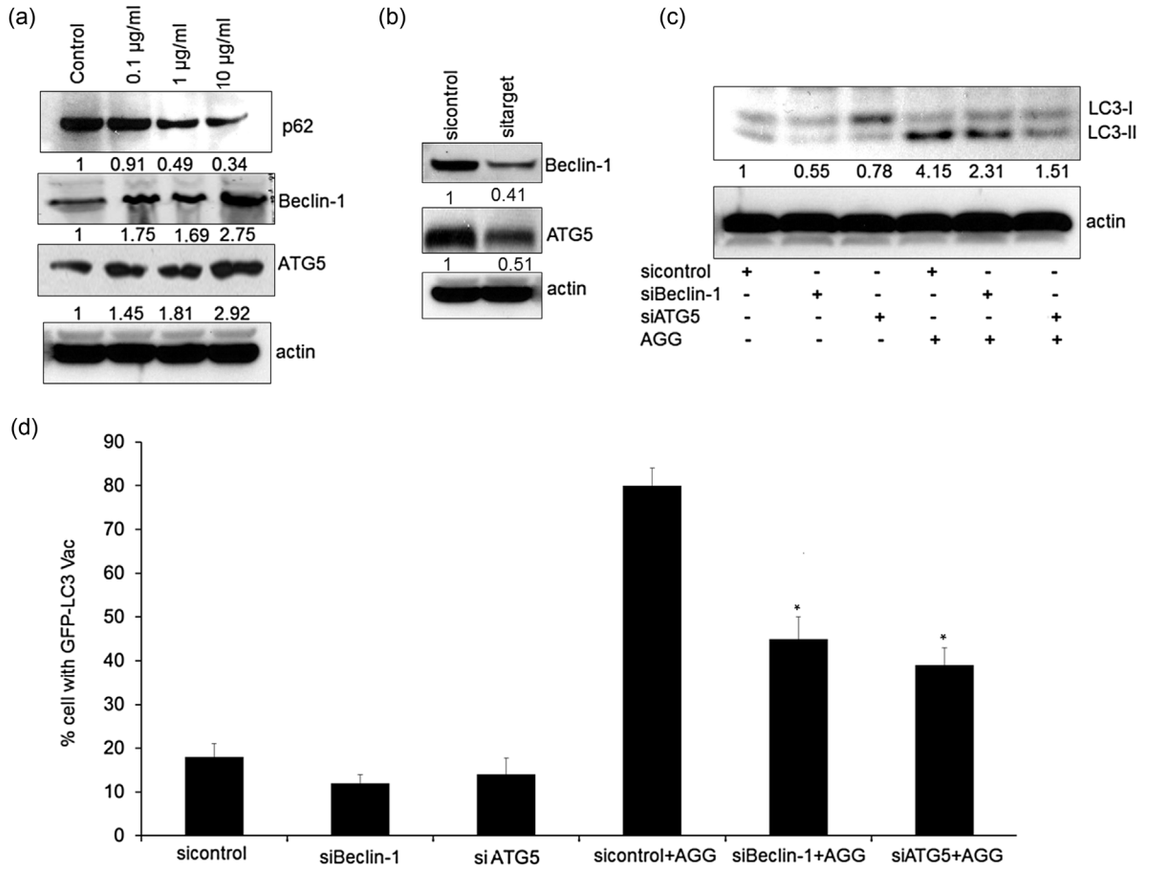

Figure 2. AGG-induced autophagic cell death was mediated through the canonical pathway. HeLa cells were treated with AGG (10 μg/ml) for 24 h and expression of p62, Beclin-1, and ATG5 were analyzed by Western blot (a). After 48 h transfection with siRNAs (b), HeLa cells were treated with AGG (10 μg/ml) for 24 h and LC3-II expression was determined Western blot (c). GFP-LC3 stable HeLa cells were transfected with the indicated siRNAs followed by AGG (10 μg/ml) treatment and cytoplasmic aggregation of GFP-LC3 was determined (d). A minimum of 100 GFP-LC3-transfected cells were counted. $^{*}P < 0.05$ compared with sicontrol-AGG. Densitometry was performed on the original blots, considering the ratio of protein to actin in control cells was 1.

(3-MA), and caspase inhibitor (Z-DEVD-FMK) and monitored the alteration in cell viability, and autophagic or the apoptotic progression. HeLa cells were pretreated with inhibitors and followed to AGG treatment for 24 h. The microscopic image showed that AGG-induced cell death and neither of the inhibitors could revert back the cell death (Figure 3a). Inhibiting apoptosis by Z-DEVD-FMK found to increase LC3 II accumulation along with a decrease in caspase 3 activity in AGG treatment (Figure 3b and c). Similarly, inhibition of autophagic cell death with 3-MA augmented AGG-induced apoptosis in HeLa cells (Figure 3b and c). In addition, AGG increased caspase activity in Beclin-1 and ATG5 deficient HeLa cells indicating that inhibition of autophagy increased the AGG-induced apoptosis and vice versa (Figure 3d and e). This study concluded that AGG simultaneously induced apoptotic and autophagic cell death.

It is well reported that AGG-induced reactive oxygen species (ROS) and is associated with apoptosis induction [11]. In the present investigation, we deciphered the role of ROS in AGG-induced autophagic cell death in HeLa cells. HeLa cells were pretreated with N-acetyl-L-cysteine (NAC; a thiol-containing antioxidant that is a precursor of reduced glutathione, 10 μM) ROS scavenger, for 2 h followed by AGG treatment for 24 h and HeLa cells were analyzed by flow cytometry and Western blot. The data showed that AGG increased the ROS generation and AGG-induced ROS generation was inhibited in the presence of NAC (Figure 4a). The Western blot analysis showed that AGG in presence of NAC decreased PARP cleavage and increased LC3-II accumulation as well as GFP-LC3 puncta formation as compared to only AGG treated group in HeLa cells (Figure 4b and c). This study concluded that AGG-dependent ROS generation induced apoptosis and inhibition of AGG-induced ROS found to switch

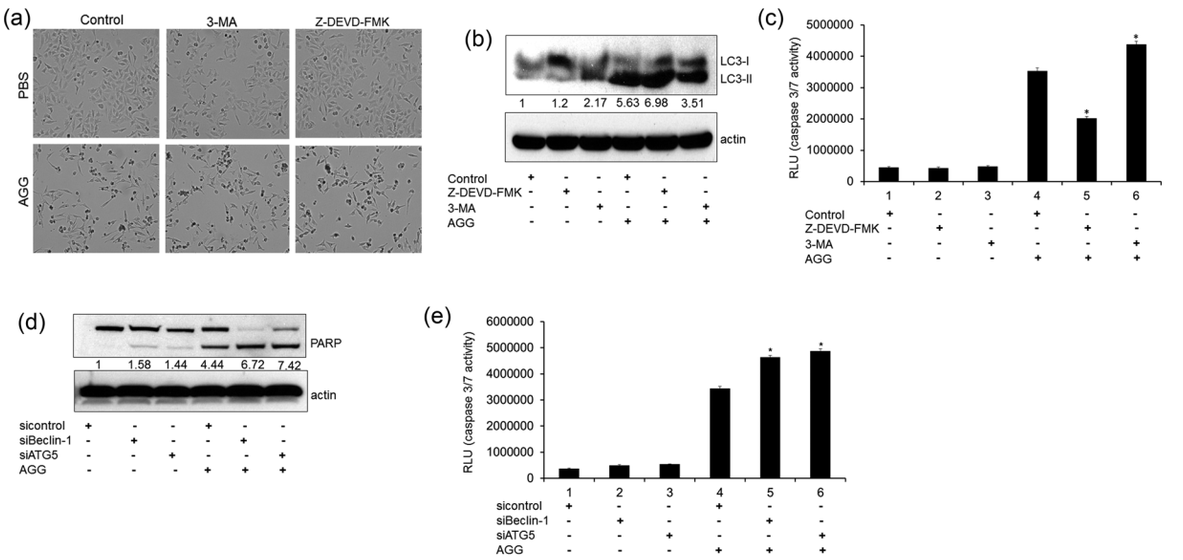

Figure 3. The relationship between AGG-induced apoptosis and autophagic cell death. HeLa cells were pretreated with PI3K-III inhibitor 3-methyladenine (3-MA) (5 μM) and caspase inhibitor (Z-DEVD-FMK) (10 μM) for 2 h followed to 24 h AGG (10 μg/ml) treatment and photographed (a), expression LC3-II was analyzed by Western blot (b) and caspase activity was measured by caspase Glo assay (c). HeLa cells were transfected with the indicated siRNAs followed by AGG treatment and PARP expression was analyzed by Western blot (d) and caspase activity was measured by caspase Glo assay (e). The values were the means ± SD of three independent experiments. *Represents statistically significant change versus AGG treated group (*$P < 0.05$). Densitometry was performed on the original blots, considering the ratio of protein to actin in control cells was 1.

from apoptosis to autophagic cell death in HeLa cells.

AGG-Induced Autophagic Cell Death in Apoptosis Deficient and Resistant Cervical Cancer Cells

To examine the role of AGG mediated autophagic death in apoptosis deficient and resistant cells, autophagic death was investigated in BAX-KD and 5-FU resistant HeLa cells. The shBax HeLa cells were characterized showing that knockdown of proapoptotic protein Bax blocks apoptosis induction by AGG (Figure 4d and e). However, AGG treated shBax Hela cells continued to exhibit higher autophagic phenotypes compared with pcDNA as evidenced by LC3-II

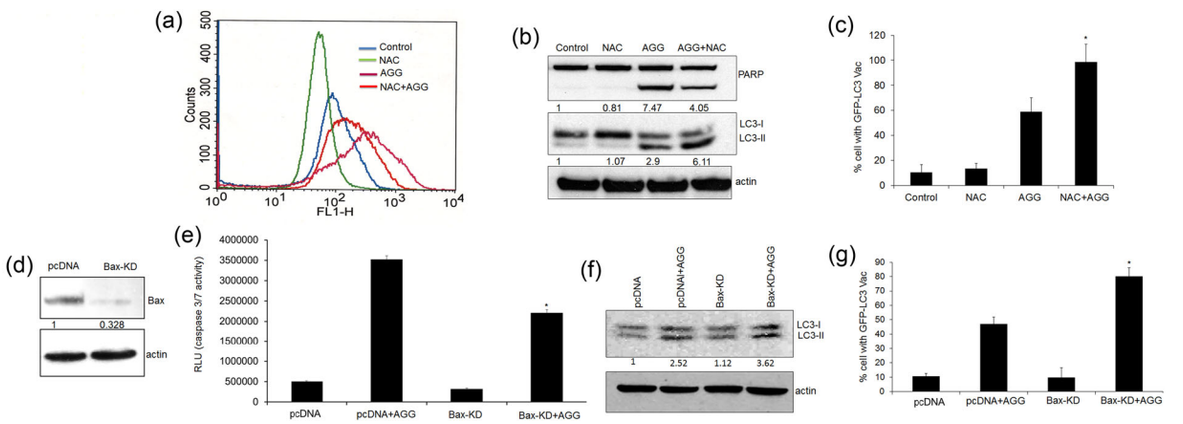

Figure 4. The role of reactive oxygen species and Bax in AGG-induced autophagic death. HeLa cells were pretreated with NAC (10 mM, 2 h) followed by AGG (10 μg/ml) for 24 h, and ROS generation was then analyzed using flow cytometry (a). HeLa cells were treated with AGG in the presence of NAC, LC3-II accumulation by Western blot (b) and GFP-LC3 puncta (c) were quantified (*$P < 0.05$, compared with only AGG treated group). HeLa cells were transfected with sh Bax for 48 h (d). After 24 h of AGG treatment, caspase3/7 activity by caspase Glo assay (e) and LC3-II expression by Western blot (f) was analyzed in sh Bax transfected HeLa cells. Stably transfected GFP-LC3 clones were transfected with sh Bax and percentage of GFP-LC3 puncta cells was examined by confocal microscopy after 24 h AGG (10 μg/ml) treatment (magnification 1000×) (g). *Corresponds statistically significant change in pcDNA-AGG (*$P < 0.05$). Densitometry was performed on the original blots, considering the ratio of protein to actin in control cells was 1.

accumulation and GFP-LC3 puncta vacuole formation (Figure 4f and g). In addition, to demonstrate the effect of AGG in resistant HeLa cells, we developed 5-FU resistant cells through continuous exposure of 5-FU to HeLa cells. Initially, we checked the cell viability against 5-FU and AGG in parent and resistant HeLa cells. It observed that there was significant increase in cell viability in 5-FU-R HeLa cells as compared to parent HeLa cells against 5-FU (Figure 5a). But we could not find any significant difference between AGG treated both parental and resistant HeLa cells (Figure 5b). Further, we examined the apoptotic and autophagic cell death in AGG treated 5-FU resistant HeLa cells. We observed there was significant decrease of apoptosis level in 5-FU-R HeLa cells compare with parent HeLa as quantified by caspase 3/7 Glo activity (Figure 5c). On the contrary, the autophagic cell death was significantly enhanced in 5-FU-R HeLa cells as to parent group as demonstrated by LC3-II accumulation and GFP-LC3 puncta vacuole formation, indicating the cell death mechanism by AGG was switched to autophagic cell death in apoptosis resistant cells (Figure 5d and e). The above findings strongly support our hypothesis that AGG could be potential alternative tumor preventive molecule to apoptotic resistant cells.

AGG-Induced Autophagic Cell Death Mediated Through PERK Dependent ER Stress

As ROS was not the regulating factor for AGG-induced autophagic death, we investigated whether endoplasmic reticulum (ER) stress might contribute to autophagic cell death through induction of ER-phagy, selective autophagy of the ER [23]. To test this hypothesis, HeLa cells were treated with AGG for different time periods and analyzed for colocalization of ER and lysosome by staining with ER-Tracker Green and LysoTracker Red as well as mitochondria and lysosome by MitoTracker Green and LysoTracker Red through a confocal microscope. The control group did not demonstrate the interaction of ER and lysosome. The treatment group showed strong colocalization of the two organelles as intense yellow color and this interaction was significantly increased in time dependent manner. These studies indicated that ER interacted with the lysosome and induced ER-phagy (Figure 6a; Supplementary Section, Figure S2). Additionally, we did not find any interaction of mitochondria and lysosome as demonstrated by confocal

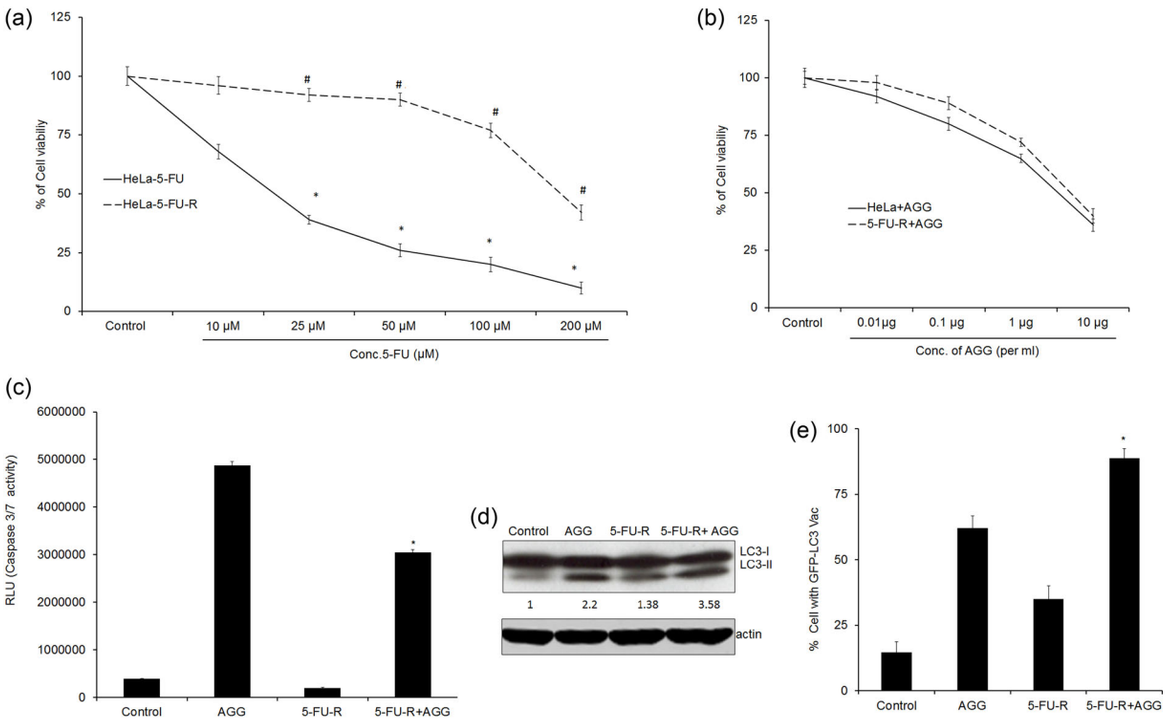

Figure 5. AGG-induced autophagic cell death in apoptosis resistant cervical cancer cells. HeLa (parent and 5-FU resistant) cells were treated with different concentration of 5-FU (a) and AGG (b) for 72 h and cell viability was performed by MTT assay. *Corresponds statistically significant change in comparison to control (*$P < 0.05$) and #Corresponds statistically significant change in comparison to 5-FU treated HeLa cells (*$P < 0.05$). After 24 h of AGG (10 µg/ml) treatment, caspase3/7 activity by caspase Glo assay (c) and LC3-II expression by Western blot (d) was analyzed in parent and 5-FU resistant HeLa cells. Transfected GFP-LC3 HeLa cells (parent and 5-FU resistant cells) were treated AGG (10 µg/ml) for 24 h and percentage of GFP-LC3 puncta cells was examined by confocal microscopy (magnification 1000×) (e). *Corresponds statistically significant change in AGG treated group (*$P < 0.05$). Densitometry was performed on the original blots, considering the ratio of protein to actin in control cells was 1.

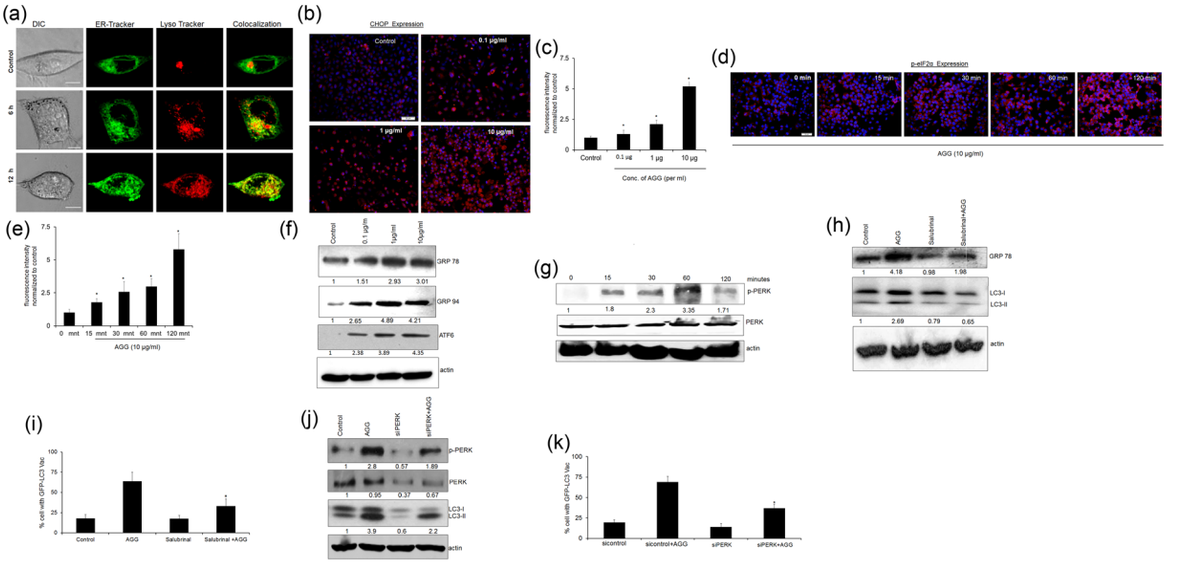

Figure 6. The role of ER stress in AGG-induced autophagic cell death. HeLa cells were treated with AGG (10 μg/ml) for indicated time periods and colocalization of ER and lysosome was analyzed with ER-Tracker Green (500 nM) and LysoTracker Red (100 nM) through confocal microscopy (a). HeLa cells were treated with AGG for indicated time periods and expression of CHOP (b and c) and p-eIF2α (d and e) analyzed by immunofluorescence microscopy (Olympus IX71, 200×, All images were quantified by using Image J) and GRP 78, GRP 94, ATF6, and p-PERK, analyzed by Western blot (f and g). *Corresponds statistically significant change in comparison to control ($^*P < 0.05$). HeLa cells were pretreated with salubrinal (5 μM) for 2 h followed by AGG treatment (10 μg/ml) for 24 h and LC3-II expression was analyzed by Western blot (h). Stably transfected GFP-LC3 clones were treated with salubrinal (5 μM) prior to AGG treatment (10 μg/ml) and autophagosome formation was quantified and data presented as a percentage of GFP-LC3 puncta cells by confocal microscopy (i). The values are expressed as the mean ± SD of three independent experiments ($^*P < 0.05$, compared with only AGG treated group). After 48 h transfection with siPERK, HeLa cells were treated with AGG (10 μg/ml) for 24 h and LC3-II expression was determined Western blot (j). GFP-LC3 stable HeLa cells were transfected with the siPERK followed by AGG (10 μg/ml) treatment and cytoplasmic aggregation of GFP-LC3 was determined (k). Densitometry was performed on the original blots, considering the ratio of protein to actin in control cells was 1.

microscopy which nullified role of mitophagy in AGG-induced autophagic cell death (Supplementary Section, Figure S2). Further, we monitored the change in ER stress regulated proteins in the presence of AGG in HeLa cells. C/EBP homologous protein (CHOP), which is commonly known as growth arrest-and DNA damage inducible gene 153 (GADD153) and expression of CHOP is the most sensitive ER stress marker, was increased expression in dose dependent manner (Figure 6b and c). Besides that, an increase in phosphorylation of eukaryotic translation initiation factor (eIF2α) in different time point after AGG treatment was observed in HeLa cells (Figure 6d and e). After 24 h AGG treatment, AGG found to increase the expression of GRP78/BiP and GRP94, the major chaperones and central regulators of unfolded protein response in dose dependent manner in HeLa cells. Besides that ATF6 one of the important ER stress sensor which induces CHOP expression was also increased in dose dependent way as shown by Western Blot (Figure 6f). Moreover, AGG increased the phosphorylation of PERK, one of the major transducers of ER stress indicating AGG-induced ER stress followed PERK mediated pathway (Figure 6g). We next determined whether AGG mediated ER stress contribute to AGG stimulated autophagy using a cell-permeable form eIF2α dephosphorylation inhibitor salubrinal, which inhibits eIF2α activity. Pretreatment of salubrinal reduced the expression of GRP78 and ER stress in AGG treated cells as compared to only AGG treated cells (Figure 6h). Intriguingly, LC3-II accumulation and percentage GFP-LC3 puncta cells were reduced after addition of salubrinal in AGG treated group as to only AGG treated HeLa cells (Figure 6h and i). Further, the role of PERK mediated ER stress by AGG was demonstrated through siRNA approach. We found that knock down of PERK significantly inhibited autophagy induction by AGG as shown by LC3-II accumulation and GFP-LC3 puncta vacuole formation (Figure 6j and k). Collectively, our data demonstrate that AGG influenced ER stress contributed to autophagy induction.

AGG Mediated Inhibition of Akt/PH Domain Promoted ER Stress-Induced Autophagic Cell Death

Akt, the active component of the phosphoinositide 3-kinase (PI3K) is well-known to contribute to the mTOR activation, which is a vital regulator of autophagy, either directly or indirectly through phosphorylation and suppression of TSC2. Akt can be activated after binding to phosphatidylinositol (3,4,5)-trisphosphate (PIP3) via its pleckstrin homology (PH) domain which controls membrane translocation, as well as phosphorylation of Thr308 in the activation loop and Ser473 in the hydrophobic domain [1,28]. In order to study, the interactions

between the PH domain and AGG, we performed a 15 ns long molecular dynamics (MD) simulation of the docked PH-AGG complex. At the end of the simulation, the complex looked to be quite stable with root mean square deviations (RMSD) value of 2 to 2.5 Å for the Cα backbone atoms (Supplementary Section, Figure S3). Hydrogen bonds formed between PH and AGG with a minimum occupancy of 40% have been summarized in the Supplementary Section Table S1. It was observed that several residues from both the PH domain (Arg15, Arg23, Arg25, Arg76, Val83, Arg86, and Thr87) and AGG (Asp109, Asp113, Asn195, Glu198, and Asn215) interface forms the H-bonds making the stable complex (Figure 7a and b). To ensure the interactions from energetics point of view, MM-PB/GBSA based binding free energies were calculated and showed in Table S2 in the Supplementary Section. It was found that the MM-PBSA-based binding free energies are larger: $-88.91\,\text{kcal mol}^{-1}$ than $-56.54\,\text{kcal mol}^{-1}$ the MM-GBSA based. The favorable contribution from the direct electrostatic interactions between PH domain and AGG was recompensed by the electrostatic desolvation free energy upon binding, which progressed to an unfavorable contribution as a whole, consistent with other MM-PB/GBSA studies [25–30]. In contrast, nonpolar interactions, $\Delta G_{\text{nonpolar}}$ (including van der Waals interactions and nonpolar solvation) contributed favorably to the binding process. Therefore, the binding of PH domain and AGG was largely compelled by intermolecular electrostatic interactions and nonpolar interactions, including the van der Waals and nonpolar solvation. Through decomposing the binding free energy into the contribution from each residue, it was likely to recognize the binding hot spots for PH domain and AGG. For PH domain, the residues Arg15, Ile19, Thr21, Arg25, Lys39, Arg76, Thr82, Val83, and Arg86 provide significant contributions (>2 kcal/mol) were basically from three anti-parallel beta sheets present and the loops connecting them. For AGG Tyr73, Asp109, Asn195, Glu198, Pro199, Asn215, Ile219, and Gln223 were recognized as hotspots basically from the active site region and adjacent areas of A chain in AGG (Figure 7c and d). To validate the in silico finding, HeLa cells were transfected with GFP-Akt-PH domain for 48 h followed to RITC labeled AGG (10 μg/ml) for 30 min and analyzed for interaction of AGG and PH domain by confocal microscopy. Overlapping of two proteins (RITC-AGG and GFP-Akt-PH) were visible showing intense yellow color with Pearson's coefficient (Rr-0.903) as well as total overlap coefficient (R-0.931) (Figure 7e).

To examine the role of AGG in Akt phosphorylation, HeLa cells were treated with AGG for different time periods and the expression of Akt was analyzed. Treatment of AGG caused significant time dependent reduction in the phosphorylation of Akt (Ser473). On the contrary, the total Akt expression remained unaltered at said time kinetics in the presence of AGG (Figure 8a). Further, AGG treatment resulted in diminished levels of the phosphorylated form of mTOR (Ser2448) without altering total mTOR (Figure 8a), revealing a potent inhibitory effect of AGG treatment on Akt/mTOR signaling. The critical role of Akt was further supported by the rescue experiment by transfecting constitutive active Akt in HeLa cells. As expected overexpression of Akt

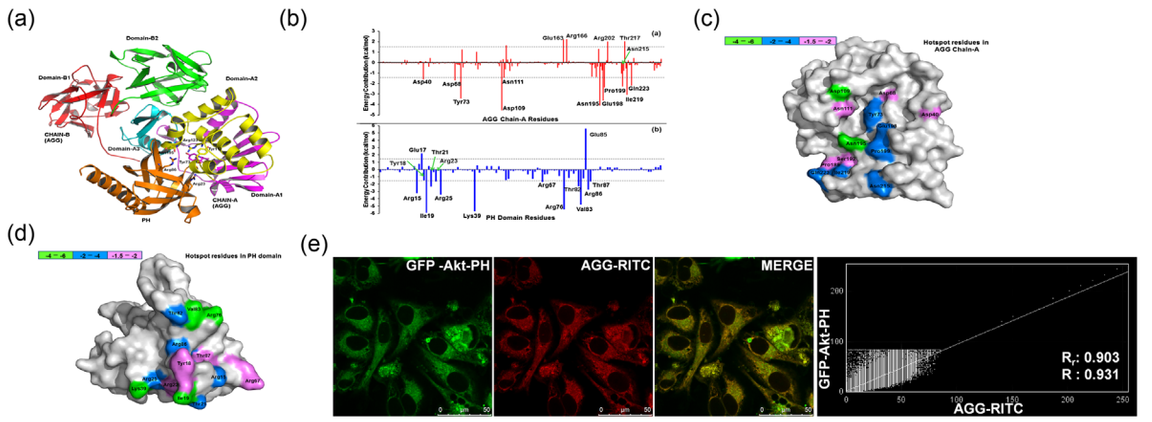

Figure 7. Interaction of Akt-PH domain and AGG. A schematic ribbon representation of the PH domain-AGG complex structure shown in different colors. The PH domain was shown in orange color while the three domains (A1, A2, and A3) in chain-A of AGG are shown in purple, yellow, and cyan colors, respectively. The two domains (B1 and B2) in chain-B of AGG are also shown in red and green colors, respectively. Few residues like Tyr73, Tyr112, and Arg123 in the active site of AGG are shown in sticks along with the residues (Arg23, Arg86, and Asn195) from the PH domain interface (a). Decomposition of ΔG on a per-residue basis or the pair interaction energy between PH domain and AGG chain-A the contribution of each residue in AGG to PH domain binding; the contribution of each residue in PH domain to AGG binding (b). Distributions of the identified hot spot residues on the PH domain surface and AGG chain-A surface. Colored bars show the range of contributions by residues in the unit kcal/mol. Chain-B for AGG protein was not shown, as it did not interact with the PH domain (c and d). Colocalization of RITC-AGG (10 μg/ml) treated and GFP-Akt-PH transfected cells was performed in confocal microscopy (magnification 630×) (Leica TCS SP8, Wetzlar, Germany) and colocalization was measured using JACoP plugin in single Z-stack sections of de-convoluted images (e).

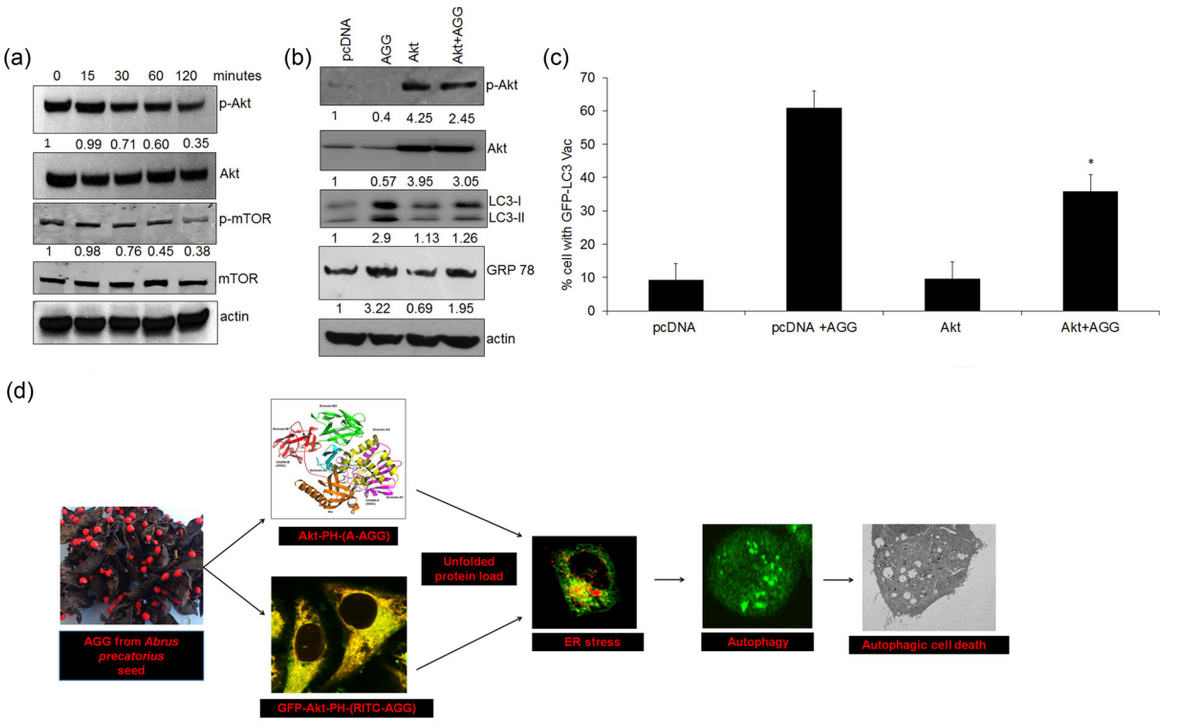

Figure 8. Akt plays a master signal for inducing autophagy by increasing ER stress. HeLa cells were treated with AGG (10 μg/ml) for different times followed by analysis of Akt and mTOR expression by Western blot (a). The expression of LC3 II and GRP 78 levels were analyzed in Akt overexpressed HeLa cells (b). Stably transfected GFP-LC3 clones were overexpressed with Akt and after AGG treatment (10 μg/ml) autophagosome formation was quantified and data presented as a percentage of GFP-LC3 puncta cells by confocal microscopy (magnification 1000×) (c). Data represented as the mean ± S.D. of three independent experiments. *Represents statistically significant change versus corresponding AGG treated group ($^*P < 0.05$). Densitometry was performed on the original blots, considering the ratio of protein to actin in control cells was 1. Schematic representation of AGG-induced ER stress mediated autophagy dependent cell death in HeLa cells (d).

interfere the AGG mediated ER stress, which was corroborated by reduced LC3-II accumulation and GFP-LC3 puncta, ultimately overcome the cell death by AGG (Figure 8b and c). Therefore, it could be firmly concluded that AGG-induced ER stress associated with autophagic cell death by inhibition of Akt through PH domain in HeLa cells (Figure 8d).

DISCUSSION

Autophagy, an alternative tumor-suppressing mechanism have evolved as a potential novel approach for cancer therapies for induction of cell death, either in addition to, or instead of, apoptosis-induced treatment. A number of studies have reported that autophagic cell death is activated in cancer cells in response to various anticancer molecules including Tamoxifen, Temozolomide (TMZ), γ-irradiation, sodium butyrate, and suberoylanilide hydroxamic acid (SAHA), arsenic trioxide (As_2O_3) [1,2]. Moreover, several clinical and preclinical studies established plant lectins including Phytohemagglutinin, Wheat germ agglutinin, Concanavalin A, *Momordica charantia* lectin, Mistletoe lectins, Soybean lectin, and Peanut agglutinin-induced autophagic cell death in different types of cancer [7,8,22,31–35]. For instance, a lectin from *Polygonatum cyrtonema*-induced apoptosis and autophagy in human melanoma A375 cells through a mitochondria-mediated ROS-p38-p53 pathway [36]. Another lectin Concanavalin A from Jack bean seeds inhibited hepatoma cells through BNIP3-mediated mitochondria autophagy [31]. Similarly, Korean mistletoe lectins, another type II ribosome-inactivating protein (RIP II) regulated self-renewal of placenta-derived mesenchymal stem cells inducing autophagy at its low concentrations. Accordingly, in the present study, we documented that AGG-induced Beclin-1 dependent autophagic cell death through ER stress in human cervical cancer cells along with apoptosis inducing potential. In addition, AGG-induced downregulation of Akt phosphorylation modulated autophagic cell death through strengthening ER stress.

In response to cancer therapy, cell death in tumor cells is induced in many ways including induction of autophagic cell death or apoptosis simultaneously, sequentially, or in a mutually exclusive manner [1,37]. Accordingly, we observed that AGG simultaneously induced apoptosis and autophagic cell death in cervical cells. Inhibition of autophagic death by

3-MA and knock down by siBeclin-1 and siATG5 significantly switched the cell death to apoptosis induced by AGG. In support, a previous study showed that several anticancer drugs (SAHA) and plant lectins induced both autophagic death and apoptosis [1,38,39]. Further, AGG induced significantly enhanced autophagic cell death in shBax transfected cells and 5-FU resistant cells indicating AGG could be very effective against apoptosis deficient and resistant cells.

Accumulating data indicate that ER stress promotes autophagy as an adaptive mechanism and upon persistent stress it can switch into cell death mechanisms, the autophagic cell death [23,40]. Our study showed that AGG found to stimulate ER stress markers including GRP78, GRP94, CHOP, and eIF2α phosphorylation through PERK dependent pathway. In this connection, GRP78, a major chaperone is considered to be the central regulator of UPR which acts as a novel obligatory component of autophagy in mammalian cells. For instance, knockdown of GRP78 inhibited autophagosome formation, which was induced by ER stress or by nutrient starvation in HeLa cells [40]. Similarly, stress dependent CHOP is important in the transcriptional activation of genes involved in the formation, elongation, and function of the autophagosome [41]. Intriguingly, we demonstrated that inhibition of ER stress with salubrinal and si PERk reduced AGG-induced autophagic cell death, suggesting a potential role of ER stress in AGG induced autophagy. In support, it was demonstrated that *Abrus* abrin-induced ER stress through stress kinases p38 MAPK to regulate apoptosis in Jurkat cells [42].

Akt can mediate cell survival and growth and its activity is regulated by phosphorylation on two regulatory residues, Thr308 in the activation loop of the catalytic domain and Ser473 in the regulatory domain. Akt inhibits autophagy through mTORC1 activation in response to growth factor stimulation [1,2,3]. The mutational Akt hyperactivation diminishes autophagy during metabolic stress, whereas Akt inhibition by different types of antitumor molecules induces autophagic cell death. Our result showed that treatment of AGG caused significant time dependent reduction in the phosphorylation of Akt (Ser473) in HeLa cells and overexpression of Akt found to suppress AGG-induced autophagic death. A previous study showed that naturally occurring agents including Concanavalin A and Plumbagin-induce autophagy by inhibiting the Akt/mTOR in cancer cells [32,43]. For the first time, AGG demonstrated to bind with PH domain of Akt through the active site region and adjacent areas, located in the cleft made by three domains of A chain preserved among the type II RIPs [12]. Apart from N-glycosidase enzymatic activity, our study documented an unknown function of A chain of AGG and AGG could be considered as non-lipid-based PH domain inhibitor which needs to be deciphered in detail. Further, how does A chain of AGG inhibit PH domain and influence Akt phosphorylation and translocation are not known. In our study, induction of ER stress through inhibition of Akt was the master signal for AGG-induced autophagic cell death. Numerous studies were available where Akt-mTOR pathway was associated with the ER stress-induced induction of apoptosis as well as autophagy [44–46]. Recently it reported that resveratrol a natural polyphenol triggers ER stress which leads to autophagic cell death in prostate cancer cells via down regulation of Akt-mTOR pathway [47]. In conclusion, the present results establish that AGG stimulated cell death by autophagy through ER stress and Akt dephosphorylation by binding with PH domain might be explored as an alternative tumor suppressor mechanism in cervical carcinoma.

ACKNOWLEDGMENTS

Authors like to acknowledge CSIR, DBT, SERB and NCI R01 for financial support to carry out this project and high performance computing facilities (ARJUN cluster) at Molecular Biophysics Unit, Indian Institute of Science, Bangalore, India. PKP is obliged to DBT and MHRD (Govt of India) for providing fellowship. BRM is a Dr. D.S. Kothari Post-Doctoral Fellow (DSKPDF), UGC, India.

REFERENCES

1. Panda PK, Mukhopadhyay S, Das DN, Sinha N, Naik PP, Bhutia SK. Mechanism of autophagic regulation in carcinogenesis and cancer therapeutics. Semin Cell Dev Biol 2015;39:43–55.
2. Bhutia SK, Mukhopadhyay S, Sinha N, et al. Autophagy: Cancer's friend or foe? Adv Cancer Res 2013;118:61–95.
3. Panda PK, Mukhopadhyay S, Sinha N, Das DN, Bhutia SK. Autophagy and apoptosis: Where do they meet? Apoptosis 2014;19:555–566.
4. Jemal A, Bray F, Center MM, Ferlay J, Ward E, Forman D. Global cancer statistics. CA Cancer J Clin 2011;61:69–90.
5. Suneja G, Bacon M, Small W Jr, Ryu SY, Kitchener HC, Gaffney DK. The cervix cancer research network: Increasing access to cancer clinical trials in low- and middle-income countries. Front Oncol 2015;5:14.
6. Dalby KN, Tekedereli I, Lopez-Berestein G, Ozpolat B. Targeting the prodeath and prosurvival functions of autophagy as novel therapeutic strategies in cancer. Autophagy 2010;6:322–329.
7. Liu Z, Luo Y, Zhou TT, Zhang WZ. Could plant lectins become promising anti-tumour drugs for causing autophagic cell death? Cell Prolif 2013;46:509–515.
8. Fu LL, Zhou CC, Yao S, Yu JY, Liu B, Bao JK. Plant lectins: Targeting programmed cell death pathways as antitumor agents. Int J Biochem Cell Biol 2011;43:1442–1449.
9. Moustapha A, Pérétout PA, Rainey NE, et al. Curcumin induces crosstalk between autophagy and apoptosis mediated by calcium release from the endoplasmic reticulum, lysosomal destabilization and mitochondrial events. Cell Death Discovery 2015;1:15017.
10. Hegde R, Maiti TK, Podder SK. Purification and characterization of three toxins and two agglutinins from *Abrus precatorius* seed by using lactamyl-Sepharose affinity chromatography. Anal Biochem 1991;194:101–109.
11. Bhutia SK, Mallick SK, Stevens SM, Prokai L, Vishwanatha JK, Maiti TK. Induction of mitochondria-dependent apoptosis by *Abrus* agglutinin derived peptides in human cervical cancer cell. Toxicol In Vitro 2008;22:344–351.

12. Bagaria A, Surendranath K, Ramagopal UA, Ramakumar S, Karande AA. Structure-function analysis and insights into the reduced toxicity of *Abrus precatorius* agglutinin I in relation to abrin. J Biol Chem 2006;281:34465–34474.
13. Ghosh D, Maiti TK. Immunomodulatory and anti-tumor activities of native and heat denatured *Abrus* agglutinin. Immunobiology 2007;212:589–599.
14. Mukhopadhyay S, Panda PK, Das DN, et al. *Abrus* agglutinin suppresses human hepatocellular carcinoma in vitro and in vivo by inducing caspase-mediated cell death. Acta Pharmacol Sin 2014;35:814–824.
15. Bhutia SK, Behera B, Das DN, et al. *Abrus* agglutinin is a potent anti-proliferative and anti-angiogenic agent in human breast cancer. Int J Cancer 2016;139:457–466.
16. Ghosh D, Bhutia SK, Mallick SK, Banerjee I, Maiti TK. Stimulation of murine B and T lymphocytes by native and heat-denatured *Abrus* agglutinin. Immunobiology 2009;214:227–234.
17. Tripathi S, Maiti TK. Stimulation of murine macrophages by native and heat-denatured lectin from *Abrus precatorius*. Int Immunopharmacol 2003;3:375–381.
18. Tripathi S, Maiti TK. Immunomodulatory role of native and heat denatured agglutinin from *Abrus precatorius*. Int J Biochem Cell Biol 2005;37:451–462.
19. Tripathi S, Maiti TK. Efficiency of heat denatured lectins from *Abrus precatorius* as immunoadjuvants. Food Agric Immunol 2003;15:279–287.
20. Bhutia SK, Mallick SK, Maiti S, Maiti TK. Antitumor and proapoptotic effect of *Abrus* agglutinin derived peptide in Dalton's lymphoma tumor model. Chem Biol Interact 2008; 174:11–18.
21. Bhutia SK, Mallick SK, Maiti TK. In vitro immunostimulatory properties of *Abrus lectins* derived peptides in tumor bearing mice. Phytomedicine 2009;16:776–782.
22. Panda PK, Mukhopadhyay S, Behera B, et al. Antitumor effect of soybean lectin mediated through reactive oxygen species-dependent pathway. Life Sci 2014;11:27–35.
23. Salazar M, Carracedo A, Salanueva IJ, et al. Cannabinoid action induces autophagy-mediated cell death through stimulation of ER stress in human glioma cells. J Clin Invest 2009;119:1359–1372.
24. Milburn CC, Deak M, Kelly SM, Price NC, Alessi DR, Van Aalten DM. Binding of phosphatidylinositol 3, 4, 5-trisphosphate to the pleckstrin homology domain of protein kinase B induces a conformational change. Biochem J 2003; 375:531–538.
25. Meher BR, Wang Y. Interaction of I50V mutant and I50L/A71V double mutant HIV-protease with inhibitor TMC114 (darunavir): Molecular dynamics simulation and binding free energy studies. J Phys Chem B 2012;116:1884–1900.
26. Meher BR, Wang Y. Binding of single walled carbon nanotube to WT and mutant HIV-1 proteases: Analysis of flap dynamics and binding mechanism. J Mol Graph Model 2012;38: 430–445.
27. Meher BR, Wang Y. Exploring the drug resistance of V32I and M46L mutant HIV-1 protease to inhibitor TMC114: Flap dynamics and binding mechanism. J Mol Graph Model 2015;56:60–73.
28. Mahadevan D, Powis G, Mash EA, et al. Discovery of a novel class of AKT pleckstrin homology domain inhibitors. Mol Cancer Ther 2008;7:2621–2632.
29. Lafont V, Schaefer M, Stote RH, Altschu D, Dejaegere A. Protein–protein recognition and interaction hot spots in an antigen–antibody complex: free energy decomposition identifies "efficient amino acids." Proteins 2007;67:418–434.
30. Zoete V, Michielin O. Comparison between computational alanine scanning and per-residue binding free energy decomposition for protein–protein association using MM-GBSA: Application to the TCR-p-MHC complex. Proteins 2007;67:1026–1047.
31. Chang CP, Yang MC, Liu HS, Lin YS, Lei HY. Concanavalin A induces autophagy in hepatoma cells and has a therapeutic effect in a murine in situ hepatoma model. Hepatology 2007;45:286–296.
32. Roy B, Pattanaik AK, Das J, et al. Role of PI3 K/Akt/mTOR and MEK/ERK pathway in Concanavalin A induced autophagy in HeLa cells. Chem Biol Interact 2014;210:96–102.
33. Zhang CZ, Fang EF, Zhang HT, Liu LL, Yun JP. Momordica charantia lectin exhibits antitumor activity towards hepatocellular carcinoma. Invest New Drugs 2015;33:1–11.
34. Choi JH, Lyu SY, Lee HJ, Jung J, Park WB, Kim GJ. Korean mistletoe lectin regulates selfrenewal of placenta-derived mesenchymal stem cells via autophagic mechanisms. Cell Prolif 2012;45:420–429.
35. Mukhopadhyay S, Panda PK, Behera B, et al. In vitro and in vivo antitumor effects of Peanut agglutinin through induction of apoptotic and autophagic celldeath. Food Chem Toxicol 2014;64:369–377.
36. Liu B, Cheng Y, Zhang B, Bian HJ, Bao JK. *Polygonatum cyrtonema* lectin induces apoptosis and autophagy in human melanoma A375 cells through a mitochondria-mediated ROS-p38-p53 pathway. Cancer Lett 2009;275:54–60.
37. Li H, Wang P, Sun Q, et al. Following cytochrome c release, autophagy is inhibited during chemotherapy-induced apoptosis by caspase 8-mediated cleavage of Beclin 1. Cancer Res 2011;71:3625–3634.
38. Liu B, Wu JM, Li J, et al. *Polygonatum cyrtonema* lectin induces murine fibrosarcoma L929 cell apoptosis and autophagy via blocking Ras-Raf and PI3K-Akt signaling pathways. Biochimie 2010;92:1934–1938.
39. Li C, Chen J, Lu B, et al. Molecular switch role of Akt in *Polygonatum odoratum* lectin-induced apoptosis and autophagy in human non-small cell lung cancer A549 cells. PLoS ONE 2014;9:e101526.
40. Li J, Ni M, Lee B, Barron E, Hinton DR, Lee AS. The unfolded protein response regulator GRP78/BiP is required for endoplasmic reticulum integrity and stress-induced autophagy in mammalian cells. Cell Death Differ 2008;15:1460–1471.
41. B'chir W, Maurin AC, Carraro V, et al. The eIF2α/ATF4 pathway is essential for stress-induced autophagy gene expression. Nucleic Acids Res 2013;41:7683–7699.
42. Mishra R, Karande AA. Endoplasmic reticulum stress-mediated activation of p38 MAPK, Caspase-2 and Caspase-8 leads to abrin-induced apoptosis. PLoS ONE 2014;9:e92586.
43. Kuo PL, Hsu YL, Cho CY. Plumbagin induces G2-M arrest and autophagy by inhibiting the AKT/mammalian target of rapamycin pathway in breast cancer cells. Mol Cancer Ther 2006;5:3209–3221.
44. Jiang H, Sun J, Xu Q, et al. Marchantin M: A novel inhibitor of proteasome induces autophagic cell death in prostate cancer cells. Cell Death Dis 2013;4:e761.
45. Jung CH, Kim H, Ahn J, et al. Anthricin isolated from Anthriscus sylvestris (L.) Hoffm. Inhibits the growth of breast cancer cells by inhibiting Akt/mTOR signaling, and its apoptotic effects are enhanced by autophagy inhibition. Evid Based Complement Alternat Med 2013;2013:385219.
46. Yu KN Chang SH, Park SJ, et al. Titanium dioxide nanoparticles induce endoplasmic reticulum stress-mediated autophagic cell death via mitochondria-associated endoplasmic reticulum membrane disruption in normal lung cells. PLoS ONE 2015;10:e0131208.
47. Selvaraj S, Sun Y, Sukumaran P, Singh BB. Resveratrol activates autophagic cell death in prostate cancer cells via downregulation of STIM1 and the mTOR pathway. Mol Carcinog 2015; 55:818–831.

SUPPORTING INFORMATION

Additional supporting information may be found in the online version of this article at the publisher's web-site.